

Evaluating the Ground Noise Footprint of Urban Air Mobility Vehicles

Teresa Moses, Michael Schmähl, Mirko Hornung

Technical University of Munich, 85748 Garching, Germany, Email: teresa.moses@tum.de

Introduction

The vision of a more sustainable aviation sector is coupled with the concept of Urban Air Mobility (UAM), which implies the deployment of electrically driven aerial vehicles within urban areas. A major challenge is the potential rise in noise exposure, as UAM designs typically feature multiple distributed rotors, leading to complex aerodynamic interactions and elevated noise emissions. To address this, numerical methods are used to predict the ground-level noise footprint of such vehicles enabling the design of noise-optimized flight routes, procedures [1, 2], and operational strategies [3]. The underlying principle for such computations is the source-path-receiver paradigm [4]. It entails the definition of noise sources and propagation mechanisms to map the noise distribution at specified observer locations. The source data is ascribed to noise hemispheres, which are based on flight test measurements [2], or computer-generated, e.g. via Blade Element Momentum Theory [3] or Computational Fluid Dynamics (CFD) [1].

To simulate a flyover, the hemispheres are strategically positioned over waypoints along a flight path, and the emitted noise on the hemisphere is then projected to ground observers, e.g., a microphone array, as visualized in Figure 1. The resulting waypoint-specific Sound Pressure Level (SPL) maps can be further converted to noise metrics, enabling the evaluation of the air taxi's acoustic footprint throughout its mission.

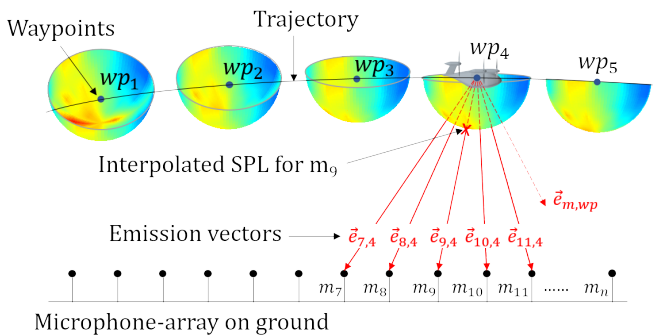


Figure 1: Illustration of the fundamental approach for acoustic ground footprint calculations of aerial vehicles. m , wp , and $\vec{e}_{m,wp}$ designate microphone, waypoint, and corresponding emission vector, respectively.

This paper presents the workflow for a noise scenario simulation environment to develop noise-conscious UAM flight routes for a tilt-rotor air taxi in cruise. The study evaluates the impact of temporal and spatial resolution on noise footprint calculations to balance accuracy and computational cost. Subsequently, the air taxi's noise signature is analyzed using single-event noise metrics to validate the algorithm and assess the effectiveness of

these metrics in evaluating UAM noise. Finally, the perceived loudness of key tones is computed to explore its potential for further noise impact assessment.

Methodology

The presented work builds on [5] that introduces the workflow and results of the acoustic analysis of a tilt-rotor air taxi at vehicle level. Therein, noise hemispheres were obtained via high-fidelity CFD simulations utilizing a hybrid acoustic analysis approach based on the Ffowcs Williams and Hawkings [6] acoustic analogy. The simulation setup was focused on capturing tonal noise sources, while broadband noise sources were not explicitly resolved. Throughout the simulation, a spherical receiver array placed around the air taxi captured the acoustic pressure over 10 rotor rotations, enabling the calculation of spectra, overall SPL, and A-weighted overall SPL (L_A) at each receiver location. The resulting hemisphere for cruising flight is depicted in Figure 2 and serves herein as input for the noise scenario calculations. Table 1 summarizes the key parameters of the tilt-rotor.

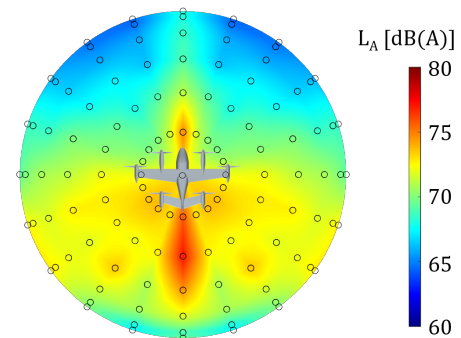


Figure 2: Noise hemisphere of the tilt-rotor in cruise, plotting the A-weighted overall SPL at 100 m observer distance as computed by [5]. The data points indicate the receiver locations used in the CFD simulation.

Table 1: Key parameters of the tilt-rotor air taxi in cruise.

Speed [m/s]	Altitude [m]	RPM [1/min]	Rotor \emptyset [m]	Weight [kg]
77.8	305	1002.5	3.3	2200

The general noise scenario calculation workflow is summarized in Figure 3. Based on the vehicle's operational parameters and prescribed trajectory, a series of waypoints is generated, each representing a quasi-static flight condition along the flight path. This waypoint data, the noise hemisphere, and a specified ground microphone array are then input into the noise scenario simulation environment. The underlying algorithm iterates through

each microphone-waypoint combination to compute the L_A -time history for every microphone throughout the air taxi's flight involving three central steps:

1. A linear interpolation across the noise hemisphere is performed to identify the L_A value projected onto each microphone. This requires computing the emission vector $\vec{e}_{m,wp}$, which represents the shortest distance between a waypoint wp and a microphone m . The corresponding emission angles are used to locate the query point on the hemisphere. It is defined by the intersection of the emission vector with the hemisphere, as marked with 'X' in Figure 1.
2. Before interpolation, the Doppler effect must be accounted for, as it shifts the perceived frequency based on the air taxi's motion relative to each microphone. This correction is applied for each microphone-waypoint combination, requiring the calculation of the relative velocity $v_{rel}(m, wp)$ from each microphone's perspective.
3. Once the Doppler-shifted noise hemisphere is positioned and oriented correctly at a waypoint, the interpolated L_A value is projected onto the corresponding ground microphone. Assuming free-field conditions and treating the air taxi as a point source, spherical spreading is applied. Thus, the projection follows the inverse square law, causing sound levels to decrease with the square of the distance from the source.

Notably, background noise, ground reflection, and atmospheric absorption were not considered in this analysis and that the noise hemisphere is based on synchronously operating rotors. Future efforts are focused on implementing the corresponding models to make the noise footprint computation even more realistic.

A key factor in noise carpet calculations is the temporal and spatial resolution, which directly impacts accuracy and computational cost. To investigate this, a convergence study was conducted. Herein, temporal resolution is determined by the number of waypoints, while spatial resolution depends on the ground microphone spacing. A straight air taxi flight over a $10 \times 10 \text{ km}^2$ area was simulated using various resolution settings. All combinations of temporal resolutions $\Delta t = [10, 5, 2.5, 1, 0.5] \text{ s}$ and spatial resolutions $\Delta s = [1000, 5000, 250] \text{ m}$ were considered. Since the acoustic impact is most pronounced directly beneath an aerial vehicle, the base microphone spacing Δs was gradually reduced towards the trajectory: from 1000 m to 500 m, it was set to $\Delta s/2$, further decreasing to $\Delta s/4$ between 500 m and 200 m, and reaching $\Delta s/8$ within 200 m of the flight path.

The influence of the resolution on the noise carpet results was evaluated by computing the maximum L_A ($L_{A,max}$). It reflects the peak noise level throughout the entire air taxi mission and is often important for regulatory and environmental assessments. The absolute deviation in $L_{A,max}$ ($\Delta L_{A,max}$) was determined for each noise carpet relative to the highest-resolution case and correlated with the computational time to assess the trade-off between

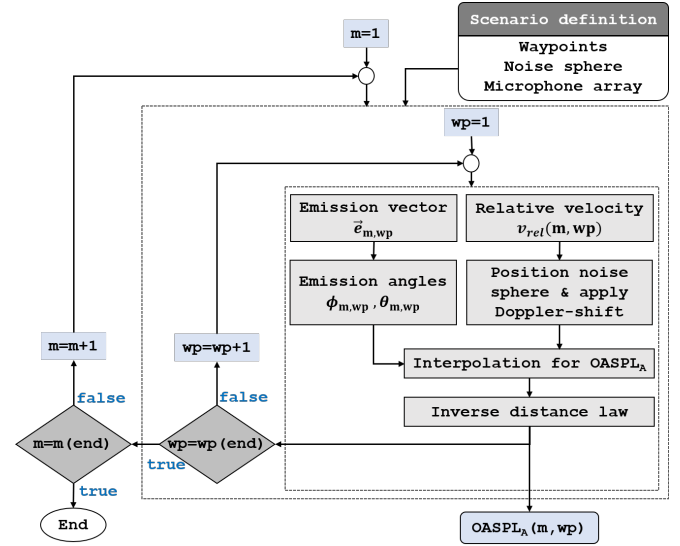


Figure 3: Noise scenario simulation environment workflow.

accuracy and efficiency. To guide the resolution selection, a dimensionless convergence ratio (CR) was defined, relating temporal and spatial resolution parameters. It is calculated as:

$$CR = \frac{v\Delta t}{\Delta s} \quad [-], \quad (1)$$

where v is the cruise speed. CR describes how far the air taxi moves within one time step relative to the spatial grid resolution. A high CR ($\gg 1$) results in poor trajectory resolution, as the air taxi moves multiple grid cells per time step. A very low CR ($\ll 1$) increases computational cost without necessarily improving accuracy. Based on the findings, a range of suitable CR values was established that reflect acceptable resolution settings. Notably, reusing computed noise carpet values for the next waypoint when operational conditions remained unchanged was not considered, but should be implemented to further reduce computational time in the future. All computations were executed on a local machine using 6 CPUs and parallel processing.

To further demonstrate the capabilities of the algorithm, an alternative trajectory with a turning radius of 2000 m was designed, simulating a fly-around of a densely populated area. Additional single-event metrics commonly used in aviation noise analysis were implemented, namely the Sound Exposure Level (SEL) and the Effective Perceived Noise Level (EPNL). The SEL represents the total sound energy of a noise event, normalized to a 1-second duration, allowing for a direct comparison between noise events with varying durations and $L_{A,max}$ [7]. The EPNL extends this by incorporating tone correction factors to assess human perception and annoyance [7]. Notably, the EPNL provides a broad evaluation of noise, considering the combined effect of multiple frequencies, fluctuations, and tonal components. However, since broadband noise was not fully resolved during the hemisphere simulations, the EPNL may not be a reliable metric in this case.

Alternatively, the equivalent perceived loudness in some

(N_{eq}) was estimated for the dominant tones in the tilt-rotor spectrum. For each microphone-waypoint combination, the SPL of the third-octave bands containing the Blade Passing Frequency (BPF) and its first four harmonics were extracted and converted to loudness in phon using equal loudness contours [8]. The resulting loudness-time histories were integrated over the noise event duration - consistent with SEL calculations - and converted to sone for a more intuitive, linear representation [7]. Summing the sone values across the bands yielded N_{eq} at each microphone. The anticipated goal was to provide a perceptually relevant metric that addresses EPNL's limitations herein by focusing on dominant tones and identifying where physically intense noise (high SPL) aligns with perceptually dominant noise (high loudness).

Results

Convergence Study

The temporal resolution analysis was conducted using the coarsest mesh with $\Delta s = 1000$ m. Figure 4a shows the $L_{A,max}$ noise carpet for $\Delta t = 10$ s, where the highest levels, as expected, are concentrated along the trajectory. The contours exhibit distinct "bubbles" at the defined waypoints, a consequence of the low temporal resolution. A higher waypoint density resulted in smoother and more continuous contours. Figure 4b plots the absolute $\Delta L_{A,max}$ between resolutions $\Delta t = 10$ s and $\Delta t = 0.5$ s. Deviations of up to ± 8 dB(A) highlight the substantial influence of temporal resolution on the results, with deviations predominantly observed in proximity to the trajectory. Consequently, a resolution of $\Delta s = 1000$ m and $\Delta t = 10$ s with corresponding CR of 0.778 lacks sufficient trajectory resolution, making a lower CR preferable.

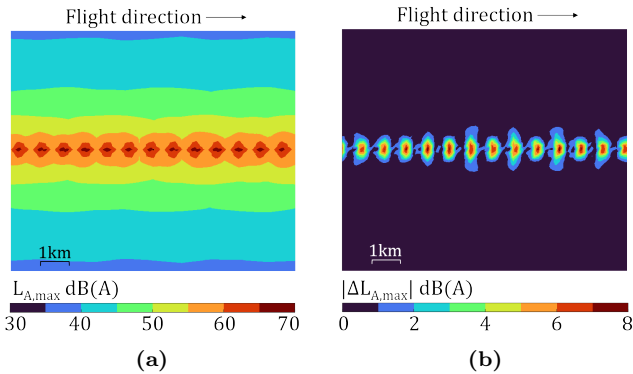


Figure 4: Noise Carpets for $\Delta s = 1000$ m displaying (a) $L_{A,max}$ for $\Delta t = 10$ s, and (b) the absolute $\Delta L_{A,max}$ between $\Delta t = 10$ s and $\Delta t = 0.5$ s.

Figure 5 summarizes the temporal resolution convergence. The left y-axis shows the percentage of the noise carpet where $\Delta L_{A,max}$ exceeds 1 dB(A) compared to the finest resolution ($\Delta t = 0.5$ s), while the right y-axis specifies computational time. Naturally, a higher waypoint count comes at the cost of a higher computational demand. Representing an optimal trade-off between computational time and accuracy, the minimum acceptable CR of 0.224 was derived from the intersection point of the two graphs. Building on this, Figure 6 plots CR values for all resolution scenarios, highlighting the approx-

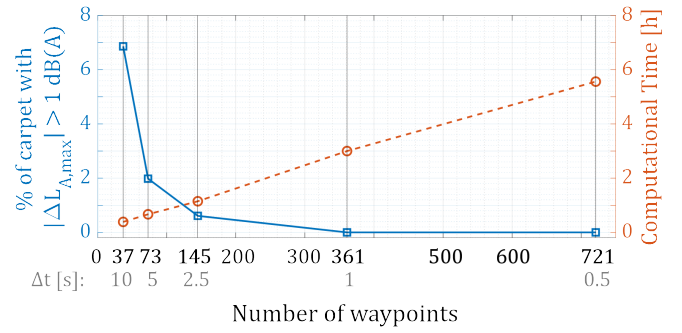


Figure 5: Temporal resolution convergence for $\Delta s = 1000$ m.

imated CR range (0.224 - 0.7) that offers an acceptable trade-off between accuracy and computational efficiency. While not shown here, it was found that the spatial resolution primarily impacts computational cost rather than improving the noise results. As Figure 5 shows, $\Delta s = 250$ m exhibits the highest CR values, indicating that the air taxi moves across multiple grid cells in a single time step. This can lead to artificial smoothing of noise contours and a loss of accuracy in the noise carpet, reinforcing the importance of maintaining CR within the identified optimal range. Ultimately, a noise carpet resolution of $\Delta t = 2.5$ s and $\Delta s = 500$ m with CR = 0.389 was chosen for subsequent simulations.

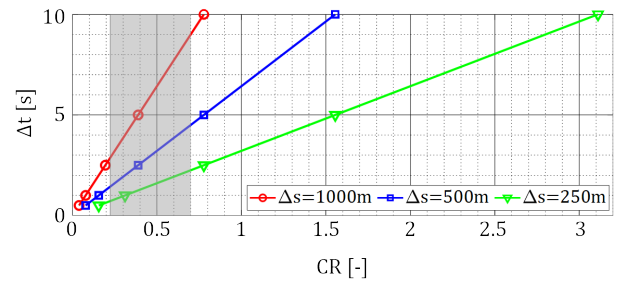


Figure 6: CRs for different resolution scenarios.

Single Event Noise Metrics

Figure 7a presents the SEL for the straight trajectory, where the air taxi flies directly over a hypothetical populated area (dashed line). Comparing these contours with those in Figure 7b, a reduction in SEL of up to 10 dB(A) is achieved by avoiding a direct flyover. Additionally, the adjusted trajectory requires the air taxi to bank up to 26° , increasing the propagation distance in the maximum noise emission direction. As a result, the SEL along the trajectory is locally reduced by 1 dB(A).

Figure 7c shows the EPNL for the alternative trajectory, revealing similar trends to Figure 7b, with the highest values concentrated along the flight path. While SEL and EPNL units are not directly comparable, both exhibit similar values within the encircled area, while tone corrections result in higher EPNL values along the trajectory. Figure 7d further supports the significant impact of tones along the trajectory, as N_{eq} for the BPF and its first four harmonics also peaks along the trajectory. It was found that first and second harmonics primarily contribute to the high N_{eq} and drive the lateral spread of noise contours. This aligns with [5], which showed

that aerodynamic interactions amplify these harmonics, making them more dominant than the BPF itself.

Generally, high N_{eq} values imply a strong perception by the human ear. Interestingly, at a horizontal distance of about 310 m from the flight path, N_{eq} already drops by half, meaning the dominant noise sources of the tilt-rotor are perceived only half as loud as directly below the trajectory. Most notably, the populated area perceives only about 1/6 of the maximum N_{eq} , suggesting that while the sound energy over time (SEL) is significant, its perceived intensity is much lower. This steep decline in perception is not visible in the EPNL carpet, indicating that high-frequency noise sources contribute to the high EPNL levels within the encircled area. This reinforces the need to include broadband noise sources when considering human perception-based noise metrics.

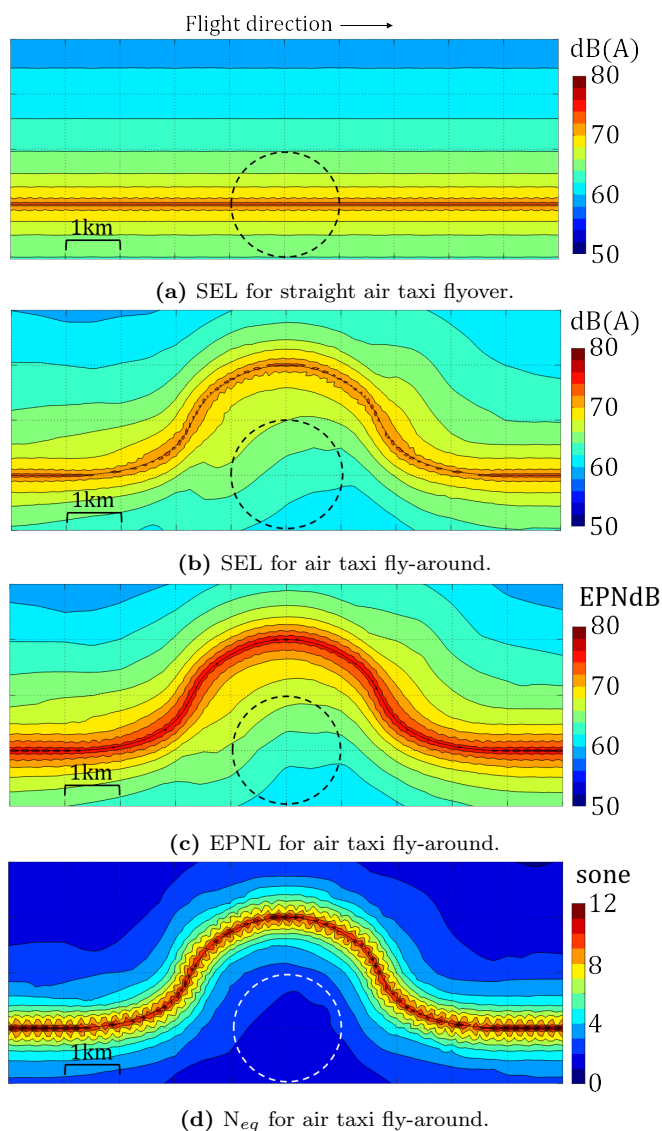


Figure 7: Noise carpet maps comparing two trajectories and multiple noise metrics.

Conclusion

This study presented a framework for simulating aviation noise scenarios. It was demonstrated that a well-balanced temporal and spatial resolution is essential to ensure re-

liable results while maintaining computational efficiency. To support the resolution selection, a dimensionless convergence ratio was introduced and a value between 0.224 and 0.7 identified as favourable. The implementation of SEL and EPNL demonstrated that rerouting an air taxi around a community can significantly reduce noise exposure. Additionally, analyzing equivalent perceived loudness for dominant tones provided insights into how physically intense noise is perceived by humans. The results showed that perceived loudness drops rapidly with distance, highlighting the disparity between physical sound levels and human perception. As sound quality metrics gain importance in aviation noise analysis, the findings suggest that excluding broadband noise from perception-based metrics is insufficient for a comprehensive assessment.

Acknowledgments

This research was conducted in connection with the Holistic Air Mobility Initiative Bavaria, a project funded by the state of Bavaria.

References

- [1] Casalino, D., van der Velden, W. C., and Romani, G., "Community Noise of Urban Air Transportation Vehicles," *AIAA Scitech 2019 Forum*, No. AIAA 2019-1834, San Diego, California, 2019.
- [2] Yin, J., Spiegel, P., and Buchholz, H., "Towards Noise Abatement Flight Procedure Design: DLR Rotorcraft Noise Ground Footprints Model and its Validation," 2004.
- [3] Pascioni, K. and Rizzi, S. A., "Tonal Noise Prediction of a Distributed Propulsion Unmanned Aerial Vehicle," *2018 AIAA/CEAS Aeroacoustics Conference*, American Institute of Aeronautics and Astronautics, June 2018.
- [4] Rizzi, S. A., Huff, D. L., Boyed, D. D., Bent, P., Henderson, B. S., Pascioni, K. A., Sargent, D. C., Josephson, D. L., Marsan, M., He, H., and Snider, R., "Urban Air Mobility Noise: Current Practice, Gaps, and Recommendations," techreport 20205007433, Langley Research Center, Hampton, Virginia, Oct. 2020.
- [5] Baerens, T., Schmahl, M., and Hornung, M., "Noise Modeling of a Tilt-Rotor Air Taxi Configuration Utilizing a Hybrid Acoustic Analogy Approach," *Proceedings of the Vertical Flight Society 80th Annual Forum*, The Vertical Flight Society, May 2024, pp. 1-17.
- [6] Ffowcs Williams, J. E. and Hawkins, D. L., "Sound Generation by Turbulence and Surfaces in Arbitrary Motion," *Philosophical Transactions of the Royal Society of London. Series A, Mathematical and Physical Sciences*, Vol. 264, No. 1151, 1969, pp. 321-342.
- [7] Sahai, A. K., Simons, D. G., and Stumpf, E., "Consideration of aircraft noise annoyance during conceptual aircraft design," 2016.
- [8] "ISO 226: 2023(E) Acoustics - Normal equal-loudness-level contours," March 2023.